



Universiteit  
Leiden  
The Netherlands

## **Histopathology of diffusion-weighted imaging-positive lesions in cerebral amyloid angiopathy**

Telgte, A. ter; Scherlek, A.A.; Reijmer, Y.D.; Kouwe, A.J. van der; Harten, T. van; Duering, M.; ... ; Veluw, S.J. van

### **Citation**


Telgte, A. ter, Scherlek, A. A., Reijmer, Y. D., Kouwe, A. J. van der, Harten, T. van, Duering, M., ... Veluw, S. J. van. (2020). Histopathology of diffusion-weighted imaging-positive lesions in cerebral amyloid angiopathy. *Acta Neuropathologica*, 139(5), 799-812.  
doi:10.1007/s00401-020-02140-y

Version: Publisher's Version  
License: [Creative Commons CC BY 4.0 license](https://creativecommons.org/licenses/by/4.0/)  
Downloaded from: <https://hdl.handle.net/1887/3184288>

**Note:** To cite this publication please use the final published version (if applicable).



# Histopathology of diffusion-weighted imaging-positive lesions in cerebral amyloid angiopathy

Annemieke ter Telgte<sup>1,2,3</sup> · Ashley A. Scherlek<sup>1</sup> · Yael D. Reijmer<sup>2,4</sup> · Andre J. van der Kouwe<sup>5</sup> · Thijs van Harten<sup>2,6</sup> · Marco Duering<sup>3,7,8</sup> · Brian J. Bacskai<sup>1</sup> · Frank-Erik de Leeuw<sup>3</sup> · Matthew P. Frosch<sup>1,9</sup> · Steven M. Greenberg<sup>2</sup> · Susanne J. van Veluw<sup>1,2</sup> 

Received: 8 November 2019 / Revised: 25 January 2020 / Accepted: 21 February 2020 / Published online: 27 February 2020  
© Springer-Verlag GmbH Germany, part of Springer Nature 2020

## Abstract

Small subclinical hyperintense lesions are frequently encountered on brain diffusion-weighted imaging (DWI) scans of patients with cerebral amyloid angiopathy (CAA). Interpretation of these DWI+ lesions, however, has been limited by absence of histopathological examination. We aimed to determine whether DWI+ lesions represent acute microinfarcts on histopathology in brains with advanced CAA, using a combined in vivo MRI—ex vivo MRI—histopathology approach. We first investigated the histopathology of a punctate cortical DWI+ lesion observed on clinical in vivo MRI 7 days prior to death in a CAA case. Subsequently, we assessed the use of ex vivo DWI to identify similar punctate cortical lesions post-mortem. Intact formalin-fixed hemispheres of 12 consecutive cases with CAA and three non-CAA controls were subjected to high-resolution 3 T ex vivo DWI and T2 imaging. Small cortical lesions were classified as either DWI+/T2+ or DWI-/T2+. A representative subset of lesions from three CAA cases was selected for detailed histopathological examination. The DWI+ lesion observed on in vivo MRI could be matched to an area with evidence of recent ischemia on histopathology. Ex vivo MRI of the intact hemispheres revealed a total of 130 DWI+/T2+ lesions in 10/12 CAA cases, but none in controls ( $p=0.022$ ). DWI+/T2+ lesions examined histopathologically proved to be acute microinfarcts (classification accuracy 100%), characterized by presence of eosinophilic neurons on hematoxylin and eosin and absence of reactive astrocytes on glial fibrillary acidic protein-stained sections. In conclusion, we suggest that small DWI+ lesions in CAA represent acute microinfarcts. Furthermore, our findings support the use of ex vivo DWI as a method to detect acute microinfarcts post-mortem, which may benefit future histopathological investigations on the etiology of microinfarcts.

**Keywords** DWI+ lesions · CAA · Post-mortem MRI · Microinfarcts · Ischemia

**Electronic supplementary material** The online version of this article (<https://doi.org/10.1007/s00401-020-02140-y>) contains supplementary material, which is available to authorized users.

✉ Susanne J. van Veluw  
svanveluw@mgh.harvard.edu

- 1 MassGeneral Institute for Neurodegenerative Disease, Massachusetts General Hospital and Harvard Medical School, 114 16th Street, Charlestown, MA 02129, USA
- 2 Department of Neurology, J. Philip Kistler Stroke Research Center, Massachusetts General Hospital and Harvard Medical School, Boston, MA, USA
- 3 Department of Neurology, Donders Institute for Brain, Cognition and Behaviour, Radboud University Medical Center, Nijmegen, The Netherlands
- 4 Department of Neurology, Brain Center Rudolf Magnus, University Medical Center Utrecht, Utrecht University, Utrecht, The Netherlands

- 5 Department of Radiology, Athinoula A. Martinos Center for Biomedical Imaging, Massachusetts General Hospital, Charlestown, MA, USA
- 6 Department of Radiology, Leiden University Medical Center, Leiden, The Netherlands
- 7 Institute for Stroke and Dementia Research (ISD), University Hospital LMU Munich, Munich, Germany
- 8 Munich Cluster for Systems Neurology (SyNergy), Munich, Germany
- 9 Neuropathology Service, C.S. Kubik Laboratory for Neuropathology, Massachusetts General Hospital and Harvard Medical School, Boston, MA, USA

## Introduction

Cerebral amyloid angiopathy (CAA) is a common type of cerebral small vessel disease (SVD) in the elderly, characterized by the deposition of amyloid  $\beta$  (A $\beta$ ) in the walls of pial arteries and cortical perforators [40]. Besides being an important risk factor for intracerebral hemorrhage (ICH), CAA is associated with a high prevalence of microinfarcts, especially in the cortex [1, 40]. Microinfarcts have been suggested as an important mechanism for vascular cognitive impairment and dementia [40]. However, studies on the role of microinfarcts in cognitive decline suffer from the limited detectability of microinfarcts in vivo [37].

One candidate approach for in vivo detection of microinfarcts is the use of diffusion-weighted imaging (DWI) [33]. Small punctate hyperintense lesions on DWI (i.e., DWI+ lesions) are frequently found in patients with CAA (15–27%) as compared to healthy older individuals ( $\leq 1.5\%$ ) [2, 3, 10, 12, 18, 36]. These DWI+ lesions, which often have a low signal on the apparent diffusion coefficient map, are thought to reflect acute (micro)infarcts [36, 37]. However, due to their subclinical nature and transient visibility up to 4 weeks after onset [28], histopathological evidence confirming the acute ischemic basis of small DWI+ lesions is still lacking, which limits their interpretation. It is especially unclear whether these DWI+ lesions represent microinfarcts that are frequently observed at neuropathological examination in cases with CAA.

In this study, we aimed to determine whether small DWI+ lesions represent acute microinfarcts in the context of CAA, using a combined in vivo MRI—ex vivo MRI—histopathology approach. First, we investigated the histopathology of a cortical DWI+ lesion observed on in vivo MRI 7 days prior to death in a CAA case, hypothesizing that it would show typical histopathologic features of an acute ischemic infarct, such as shrunken, eosinophilic and pyknotic neurons with no or only early glial inflammatory response [22, 30]. Second, we assessed the use of ex vivo DWI to detect acute microinfarcts post-mortem in intact hemispheres of 12 consecutive cases with CAA, and explored factors associated with their occurrence, including demographics, ICH as cause of death and post-mortem characteristics.

## Methods

The study was embedded in an ongoing ex vivo MRI—histopathology study at the Massachusetts General Hospital (MGH), aimed at investigating the etiology of microvascular lesions in CAA [35, 38, 39]. Study approval was obtained from the MGH's institutional review board [39].

## Cases

To investigate the histopathology of an in vivo DWI+ lesion (objective 1), one female case with definite CAA [9], and an in vivo cortical DWI+ lesion identified on clinical MRI performed 7 days prior to death at age 87 were included from a previous study [35]. As part of this previous study, five contiguous coronal brain slabs (0.5–1.0 cm thick) from the left occipital lobe (including the DWI+ lesion location) were subjected to ex vivo MRI. Slabs were fixed and scanned in 10% formalin.

To assess the use of ex vivo DWI to detect acute microinfarcts post-mortem in intact hemispheres (objective 2), 13 cases with clinically possible or probable CAA (according to the modified Boston criteria [9]) were included. Cases were either enrolled through an ongoing brain donation program led by the MGH hemorrhagic stroke research group or came to autopsy through the MGH's neuropathology service. The cerebral hemisphere least affected by recent hemorrhages was selected for ex vivo scanning. On routine neuropathological examination performed on the other hemisphere, definite CAA was confirmed in 12 cases [9]. The other case with no CAA on pathology was included as a control case. In addition, two other consecutive control cases without neurological disease were included from the local MGH neuropathology service, for which one hemisphere was randomly selected. Informed consent was obtained prior to autopsy from a legal representative or next of kin [38, 39]. After fixation in 10% formalin for at least 4 weeks, each intact hemisphere was vacuum packed in periodate-lysine-paraformaldehyde (PLP) and kept at 4 °C. One day prior to the ex vivo MRI the cerebral hemispheres were kept at room temperature, and any remaining air bubbles were removed prior to scanning. The cerebral hemispheres were cut in 1.0 cm-thick coronal slabs after scanning.

Finally, to verify the ability of ex vivo DWI to detect the presence of DWI+ lesions post-mortem (objective 3), we included two intact contiguous coronal brain slabs (each ~ 1 cm thick) of a 30-year old non-CAA case with multiple small cortical and subcortical DWI+ lesions on MRI performed < 2 weeks prior to death (Supplementary material). Because of the presence of DWI+ lesions on in vivo MRI, we considered this case as our positive control case. A flow chart summarizing the three study objectives can be found in the Supplementary material (Supplemental Fig. 2).

## Ex vivo MRI protocol and image processing

To guide sampling of the identified in vivo DWI+ lesion in a previously reported CAA case we used T2-weighted turbo-spin echo (TSE) images that had been acquired on a 7 T MRI scanner (MAGNETOM, Siemens Healthineers,

Erlangen, Germany) equipped with a 32-channel head coil [sequence parameters:  $0.3 \times 0.3 \times 0.3 \text{ mm}^3$  voxels, repetition time (TR) 1000 ms, echo time (TE) 63 ms, flip angle  $120^\circ$ , turbo factor 9, acquisition time  $\sim 1 \text{ h}$ ] [35].

The whole hemispheres were scanned overnight on a 3 T MRI scanner (MAGNETOM Trio, Siemens Healthineers, Erlangen, Germany) equipped with a 32-channel head coil. Amongst others, the protocol included a high-resolution diffusion-weighted gradient-echo true fast imaging with steady-state free precession sequence [21] (True FISP,  $1.0 \times 1.0 \times 1.0 \text{ mm}^3$  voxels, 44 diffusion-weighted directions, estimated effective  $b$  value  $\sim 1000 \text{ s/mm}^2$ , 8  $b=0$  images, TR 29.77 ms, TE 23.89 ms and acquisition time  $\sim 8 \text{ h}$ ). A steady-state free precession sequence is preferred over a spin echo echo-planar imaging sequence, when imaging an entire brain or whole hemisphere, due to a drop in the diffusion coefficient and T2 relaxation times in fixed tissue [21]. Furthermore, the protocol included a T2-weighted TSE sequence ( $0.5 \times 0.5 \times 0.5 \text{ mm}^3$  voxels, TR 1800 ms, TE 61 ms, flip angle  $150^\circ$ , turbo factor 15, acquisition time  $\sim 3 \text{ h}$ ).

Raw images were converted to 3D volumes using FreeSurfer (<https://surfer.nmr.mgh.harvard.edu/>) [4].

Ex vivo diffusion data were corrected for motion, signal drift and eddy currents and mean diffusivity maps were generated using ExploreDTI (<http://www.exploredti.com>) [19]. Subsequently, diffusion-weighted trace images were calculated based on the geometric mean across diffusion directions. To account for the difference in resolution between the DWI and 3 T T2 scans, we down sampled the T2 scans to a  $1.0 \text{ mm}^3$  isotropic resolution using FLIRT within the Functional Magnetic Resonance Imaging of the Brain (FMRIB) Software Library (FSL; v5.0) [14].

### Ex vivo image analysis

Utilizing MRIcron (<https://www.nitrc.org/projects/mricron>), one rater (AtT), who was blinded for clinical characteristics, screened the diffusion-weighted trace images for hyperintense, cortical lesions  $< 5 \text{ mm}$  in diameter (i.e., DWI+ lesions), as previously defined [37]. A second rater (SJvV) assessed the same scans. Cohen's kappa was 0.73 (95% CI 0.39–1.00) and Dice similarity coefficient was 0.67, indicating good inter-rater agreement. Using a previously developed in-house tool in MeVisLab (MeVis Medical Solutions AG, Bremen, Germany), one rater (SJvV) screened the T2 0.5 mm resolution scans for hyperintense cortical lesions  $< 4 \text{ mm}$  in diameter (i.e., T2+ lesions) [39]. Previously, it has been demonstrated that these lesions correspond to microinfarcts on histopathology [35, 37, 39]. Rating of the T2 scans had been performed in the context of a previous study on microinfarcts [39], and as such was done independently of the DWI scans. Subsequently, the DWI and T2 ratings were combined in MeVisLab, resulting in a

set of DWI+/T2+ lesions (presumed acute cortical microinfarcts), and DWI–/T2+ lesions (presumed chronic cortical microinfarcts). Finally, per case the lesion annotations were projected on whole-hemisphere surface renderings to allow for a qualitative assessment of the topographical distribution of DWI+/T2+ vs. DWI–/T2+ lesions throughout the brain.

Three CAA cases with many cortical microinfarcts on T2 were selected for further histopathological analysis. A subset of representative and isolated DWI+/T2+ and DWI–/T2+ lesions was selected. Care was taken to include enough anatomical landmarks in the sampled tissue blocks to enhance successful lesion retrieval. To avoid potential selection bias due to the difference in resolution between the DWI and T2 scans, we only targeted DWI–/T2+ lesions for histopathology that were also visible on the down sampled  $1.0 \text{ mm}^3$  T2 scan.

### Histopathological analysis

Serial  $6 \mu\text{m}$ -thick sections stained for hematoxylin & eosin (H&E) and glial fibrillary acidic protein (GFAP), collected within a previous study, were assessed to determine the histopathological features of the in vivo DWI+ lesion observed in a CAA case from that study [35].

Ex vivo DWI+/T2+ and DWI–/T2+ lesions were, guided by the T2 scan, localized on the brain slabs and sampled within tissue blocks measuring  $2.0 \times 1.0 \times 0.5 \text{ cm}$ , corresponding to the size of a standard tissue cassette. The depth of the lesion within the block was estimated. Samples were dehydrated overnight through immersion in graded series of ethanol and embedded in paraffin and cut on a microtome into  $6 \mu\text{m}$ -thick sections. More specifically, at the estimated lesion depth we alternately collected six sections on a glass slide and skipped the next 30 sections, until we were sure the entire lesion was captured. The first sections of each series of six were stained for H&E using standard histology protocols. On adjacent sections, bright field immunohistochemistry was performed for GFAP to detect reactive astrocytes (rabbit, G9269; Sigma St Louis, MO; 1:1000) following previously described protocols [38, 39], and Cluster of Differentiation 68 to detect reactive microglia/macrophages (CD68, mouse, GA609; Dako, Santa Clara, CA; 1:500) using a fully automated stainer (Bond Rx, Leica). A Perls' iron stain was included to assess the presence of iron deposits. All stained sections were scanned on the NanoZoomer™ whole slide scanner (Hamamatsu Photonics K. K., Japan) using a  $20\times$  objective, and the obtained images were assessed using the NDP.view2 viewing software (version 2.7.39). Sections containing the core of the lesion were included in the analysis and used to assess the pathological features and lesion size (largest diameter in  $\mu\text{m}$  as measured on H&E at  $2.5\times$  magnification).

Lesions were defined as acute microinfarcts if on H&E they were characterized by a focal area of tissue pallor containing eosinophilic (“red”) neurons, in combination with no or only minimal reactive astrocytes in the lesion periphery based on GFAP immunohistochemistry. Chronic microinfarcts were defined as areas of tissue loss with “puckering” or cavitation, without evidence of eosinophilic neurons on H&E, together with many reactive astrocytes in the lesion periphery based on GFAP. In addition to these core pathological findings, we assessed all microinfarcts for evidence of reactive microglia/macrophages with CD68 staining and hemosiderin deposits with Perls’ iron, which are both indicative of subacute to chronic microinfarcts. In case of uncertainty, microinfarcts were discussed with a board-certified neuropathologist (MPF) blinded to MRI and clinical data, and the study hypothesis. Subsequently, to assess the performance of ex vivo DWI to detect acute microinfarcts post-mortem, we performed a retrospective analysis in which the included sections were assessed for additional microinfarcts. For these microinfarcts we reported their pathological features, size as measured on H&E and appearance on the ex vivo DWI, T2 0.5 mm<sup>3</sup> and T2 1.0 mm<sup>3</sup> scans.

### Statistical analysis

We compared data on the presence and number of DWI+/T2+ and DWI–/T2+ lesions and demographics between the CAA and control cases using Mann–Whitney *U* test for continuous outcome variables and Fisher’s exact test for categorical outcome variables. Using Spearman correlation, the relationship between the number of DWI+/T2+ and DWI–/T2+ lesions was assessed. Within cases with CAA, we explored associations between the number of DWI+/T2+ lesions and demographic, clinical and ex vivo MRI characteristics using Spearman correlation or Mann–Whitney *U* test. To evaluate the performance of ex vivo DWI to detect acute microinfarcts post-mortem, we calculated its classification accuracy (total number of correct predictions/total number of predictions) and performed a sensitivity and specificity analysis using MEDCALC ([https://www.medcalc.org/calc/diagnostic\\_test.php](https://www.medcalc.org/calc/diagnostic_test.php)). Statistical analyses were performed in R (version 3.5.3; <https://www.R-project.org>), and  $\alpha$  was set at 0.05, two-tailed.

## Results

### Histopathology underlying in vivo DWI+ lesion

Results on the histopathological analysis of the cortical DWI+ lesion detected on in vivo MRI 7 days before death in a CAA case are shown in Fig. 1. On the high-resolution ex vivo T2 scan a hyperintense lesion was detected, possibly

corresponding to the in vivo DWI+ lesion. On H&E, the corresponding area was characterized by tissue pallor and showed evidence of eosinophilic neurons. The adjacent GFAP stained section revealed no severe astrogliosis, implying that recent ischemic injury had occurred in this area.

### Ex vivo MRI observations

Because of the relatively low spatial resolution of in vivo DWI, we subsequently explored DWI+ lesions on high-resolution ex vivo DWI as a more reliable and direct way to investigate the histopathology of DWI+ lesions. Evaluating the ex vivo 3 T DWI and T2 scans, a total of 130 DWI+/T2+ lesions were identified in 10/12 (83%) cases with CAA (Table 1). The median [IQR] number of ex vivo DWI+/T2+ lesions was 1.5 [1.0–6.75]. In contrast, no ex vivo DWI+/T2+ lesions were observed in control cases ( $p=0.022$ ). Since cases with CAA were significantly younger than controls ( $p=0.014$ ), the increased DWI+/T2+ lesion burden in CAA cases relative to controls could not be attributed to increased age. DWI–/T2+ lesions (total number of 370) were present in all CAA and control cases, though the number of these lesions was significantly higher in cases with CAA (median 23.5 vs. 3.0,  $p=0.030$ ). The number of DWI+/T2+ and DWI–/T2+ lesions was positively correlated (Spearman  $\rho=0.84$ ,  $p<0.001$ ). Furthermore, within cases, DWI+/T2+ lesions showed a similar topographical distribution throughout the brain as the DWI–/T2+ lesions, suggesting a shared pathogenesis between these lesions (Fig. 2).

Subsequently, we explored factors associated with the number of ex vivo DWI+/T2+ lesions among cases with CAA. Higher age at death tended to be related to more ex vivo DWI+/T2+ lesions (Spearman  $\rho=0.49$ ,  $p=0.109$ ). Sex, ICH as cause of death and global CAA severity score were all not associated with the number of DWI+/T2+ lesions (smallest  $p=0.326$ ). A longer post-mortem interval tended to be related to fewer DWI+/T2+ lesions (Spearman  $\rho=-0.58$ ,  $p=0.133$ ), whereas a longer fixation duration was associated with more DWI+/T2+ lesions (Spearman  $\rho=0.60$ ,  $p=0.039$ ).

### Histopathology underlying ex vivo DWI+/T2+ and DWI–/T2+ lesions

Cases 1, 2 and 4 were selected for histopathological analysis, because of the presence of many ex vivo T2+ lesions (Table 2). Across these cases, ten representative DWI+/T2+ and seven DWI–/T2+ lesions were targeted for histopathological analysis. Of these, eight (80%) and five (71%) lesions were successfully retrieved, respectively. The remaining four lesions could not be retrieved due to erroneous sampling.

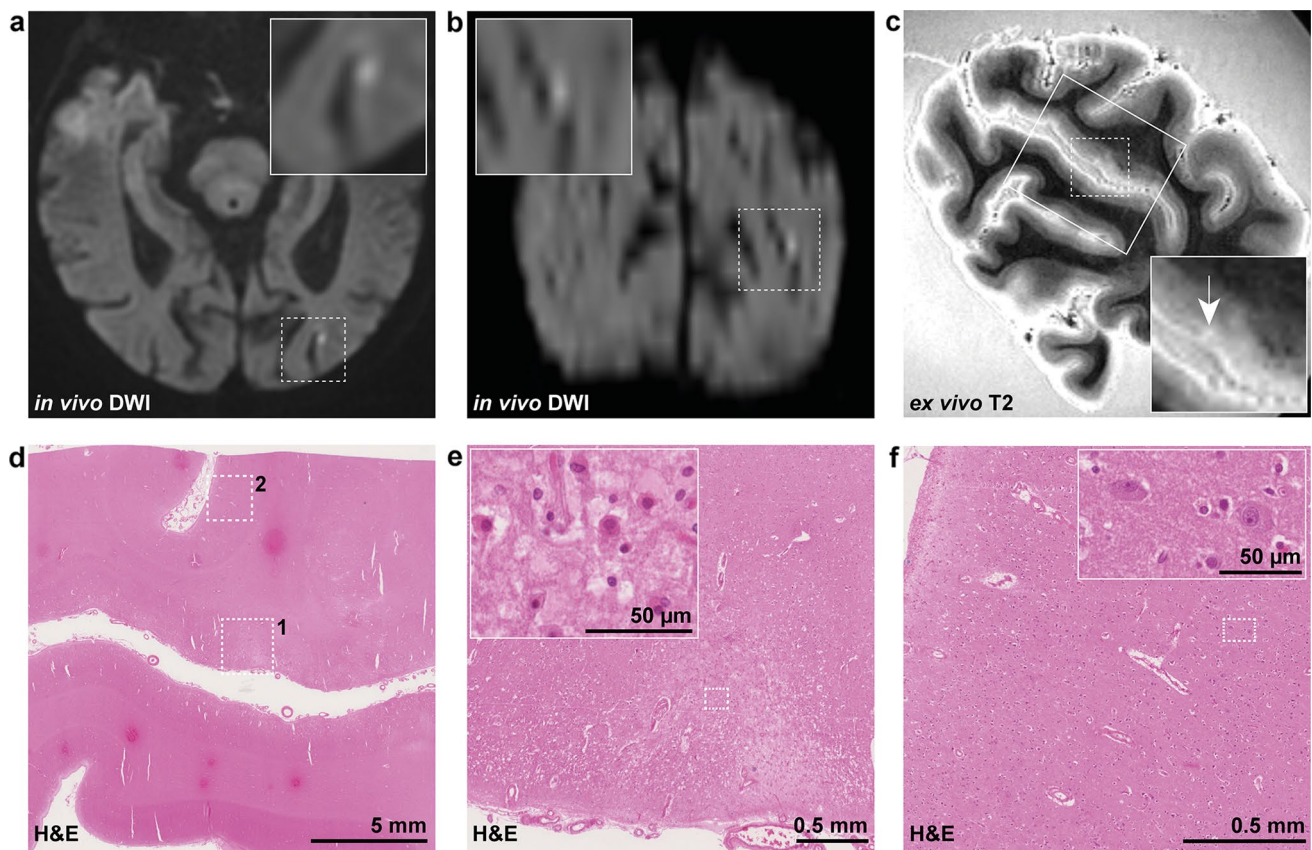


**Fig. 1** Histopathological verification of an in vivo DWI+ lesion in CAA. An in vivo cortical DWI+ lesion was detected in the left occipital lobe of a case with CAA on clinical MRI 7 days before death (**a** axial view, **b** coronal view). Five coronal slabs covering this region were subjected to high-resolution 7 T ex vivo T2 to guide tissue sampling as part of a previous study [35], and a T2 hyperintense lesion which may correspond to the in vivo DWI+ lesion was identified (**c** white arrow). A small tissue block (outlined on T2 with rectangle)

was cut and subjected to H&E staining (**d**). On H&E, a focal area of tissue pallor (dotted square 1) was identified with evidence of eosinophilic necrosis (inset in **e**), indicative of recent ischemia. In a control cortical area nearby (dotted square 2 in **d**) no evidence of eosinophilic necrosis was seen (**f**). Note that the chance for a false-positive finding was high in this case, owing to the large difference in resolution between in vivo and ex vivo MRI. *DWI* diffusion-weighted imaging, *H&E* hematoxylin & eosin

**Table 1** Group characteristics

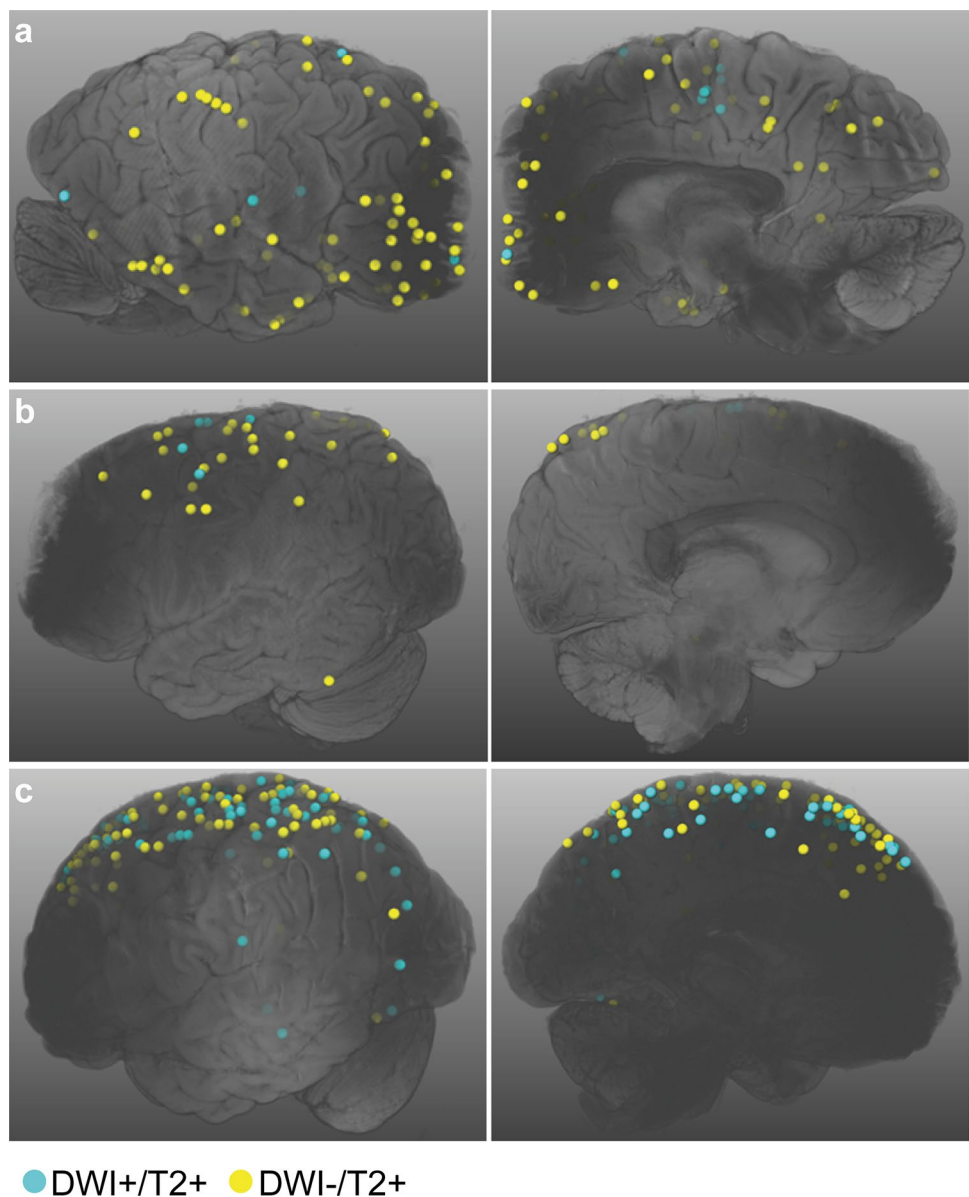
	CAA <i>n</i> = 12	Controls <i>n</i> = 3	<i>p</i>
<b>Demographics</b>			
Age, years	70 [67–79]	90 [89–93]	0.014
Sex, <i>M</i>	8 (67%)	1 (33%)	0.525
<b>Ex vivo DWI+/T2+ lesions</b>			
Presence, <i>Y</i>	10 (83%)	0 (0%)	0.022
Number	1.5 [1.0–6.75]	0 [0–0]	0.031
<b>Ex vivo DWI–/T2+ lesions</b>			
Presence, <i>Y</i>	12 (100%)	3 (100%)	–
Number	23.5 [8.5–30.5]	3.0 [2.0–4.5]	0.030

Data present median [IQR] or number (%)

On microscopic examination, all eight DWI+/T2+ lesions proved to be acute cortical microinfarcts as reflected by a focal area of tissue pallor containing eosinophilic neurons on H&E and absence of or only mild reactive astrocytes in the lesion periphery based on GFAP staining (Fig. 3). On CD68, no or fragmented (“beaded”) microglia were observed. All DWI+/T2+ lesions were negative for iron. The median [IQR] lesion size as measured on H&E was 2.35 mm [1.72–3.10] (in greatest diameter). On the ex vivo mean diffusivity map of the eight DWI+/T2+ lesions, assessed in retrospect in a consensus meeting between two raters (AtT, SJvV), two appeared hypointense, five isointense, and one somewhat hyperintense.

The five DWI–/T2+ lesions demonstrated a mixed histopathology. Three lesions (0.84, 1.86, and 2.23 mm) were characterized by a focal area of tissue loss or a central cavitation on H&E, and many reactive astrocytes in the

**Fig. 2** Topographical distribution of ex vivo DWI+/T2+ and DWI-/T2+ lesions. Shown are the whole hemisphere surface renderings of the cases selected for the histopathological analysis (a–c correspond to cases 1, 2, and 4 in Table 2, respectively). Within cases, DWI+/T2+ and DWI-/T2+ lesions show a similar topographical distribution throughout the brain. DWI diffusion-weighted imaging



lesion periphery based on GFAP, indicative of chronic cortical microinfarcts (Fig. 4). The lesions exhibited only few reactive or amoeboid microglia on CD68, but contained some iron-positive deposits, due to the presence of superficial siderosis nearby in one. Two lesions appeared hyperintense on the mean diffusivity map and one isointense. In contrast, the two other DWI-/T2+ lesions (0.56 and 1.94 mm) were suggestive of acute cortical microinfarcts, as indicated by the presence of eosinophilic neurons, and only mild GFAP positivity. Both lesions were almost negative for CD68, negative for iron and isointense on the mean diffusivity map. In retrospect, the DWI signal corresponding to these lesions was subtly increased.

#### **Analysis of additional cortical microinfarcts identified on microscopy**

Upon microscopic examination of the sections included in the abovementioned analysis ( $n = 12$  sections), we found an additional 19 cortical microinfarcts (0.63 mm [0.43–1.19]). Of these, two lesions (0.92 and 4.41 mm) represented acute cortical microinfarcts. However, in retrospect both microinfarcts were not visible on ex vivo DWI or T2, possibly due to the small size and a scan artifact (i.e., an air bubble at the site of the lesion), respectively. The remaining 17 lesions were all older cortical microinfarcts. Interestingly, among these older microinfarcts variation was observed in the morphology and concentration

**Table 2** Case description

Case ID	Sex	Age at death (years)	Cause of death due to acute ICH	PMI (h)	Fixation duration (days)	3 T ex vivo DWI+/T2+ lesions	3 T ex vivo DWI-/T2+ lesions	CAA severity score	Other neuropathological findings
Objective 1: histopathology of in vivo DWI+ lesion in CAA									
1	F	87	Unk	Unk	2469	n/a	n/a	Vonsattel 3 [35]	Braak and Braak stage III, moderate hypertensive cerebrovascular disease pathology [35]
Objective 2: histopathology of ex vivo DWI+ lesions in CAA									
Cases									
1	M	80	No	Unk	476	12	103	5	A3B3C2
2	M	70	Yes	16	377	5	29	9	A3B3C1, moderate hypertensive vasculopathy
3	M	76	No	27	43	1	20	7	A3B3C2, arteriolosclerosis
4	M	65	Yes	14	498	74	83	7	A3B1C2
5	M	81	No	Unk	69	2	11	5	A3B2C2, moderate arteriolosclerosis
6	F	70	No	Unk	71	1	7	6	A3B1C1, mild arteriolosclerosis
7	M	67	No	Unk	50	1	9	10	A3B3C2
8	M	69	Yes	36	27	1	4	10	A3B1C2, mild arteriolosclerosis
9	F	64	Yes	30	28	0	3	8	A3B2C3
10	F	79	Yes	37	153	2	29	8	A3B3C2
11	M	67	No	24	79	0	27	5	A3B1C1, moderate arteriolosclerosis
12	F	88	Yes	11	50	31	35	8	A2B3C2
Controls									
13	M	90	No	6	58	0	3	0	A2B1C2, mild hypertensive disease
14	F	95	No	4	45	0	1	0	A1B2C0
15	F	88	No	9	136	0	6	0	A2B1C1, globular glial tauopathy, mild to moderate arteriolosclerosis
Objective 3: positive control									
1	F	30	No	19	1278	10	13	0	Diffuse and extensive microinfarcts (ranging from hours to weeks old) of the white and grey matter

After an independent rating of the lower resolution DWI (1.0 mm<sup>3</sup>) and high-resolution T2 (0.5 mm<sup>3</sup>) scans, the annotations were combined resulting in a set of DWI+/T2+ and DWI-/T2+ lesions. Notably, DWI+ lesions that did not correspond to a cortical microinfarct on T2 were excluded ( $n=6$  lesions), whereas DWI+ lesions that did correspond to a cortical microinfarct on T2, but were overlooked during rating, were added to the final dataset ( $n=20$  lesions). In case of uncertainty, discrepancies were resolved in a consensus meeting between both raters. Fixation duration was calculated as the number of days between death and the ex vivo MRI scan. The CAA severity score represents a cumulative cortical CAA score which was calculated on the basis of A $\beta$  stained sections retrieved from four predefined areas, including the frontal, temporal, parietal and occipital cortex. Each section was scored as follows: 0 (absence of CAA), 1 (scant A $\beta$  deposition), 2 (some circumferential A $\beta$ ), or 3 (widespread circumferential A $\beta$ ) [20, 39]. Neuropathology findings in addition to CAA were retrieved from the neuropathology reports after routine neuropathological examination of the other cerebral hemisphere. The ABC score represents the NIA-Alzheimer Association score for Alzheimer's Disease neuropathologic changes [13]. *ICH* intracerebral hemorrhage, *n/a* not applicable, *PMI* post-mortem interval, *Unk* unknown



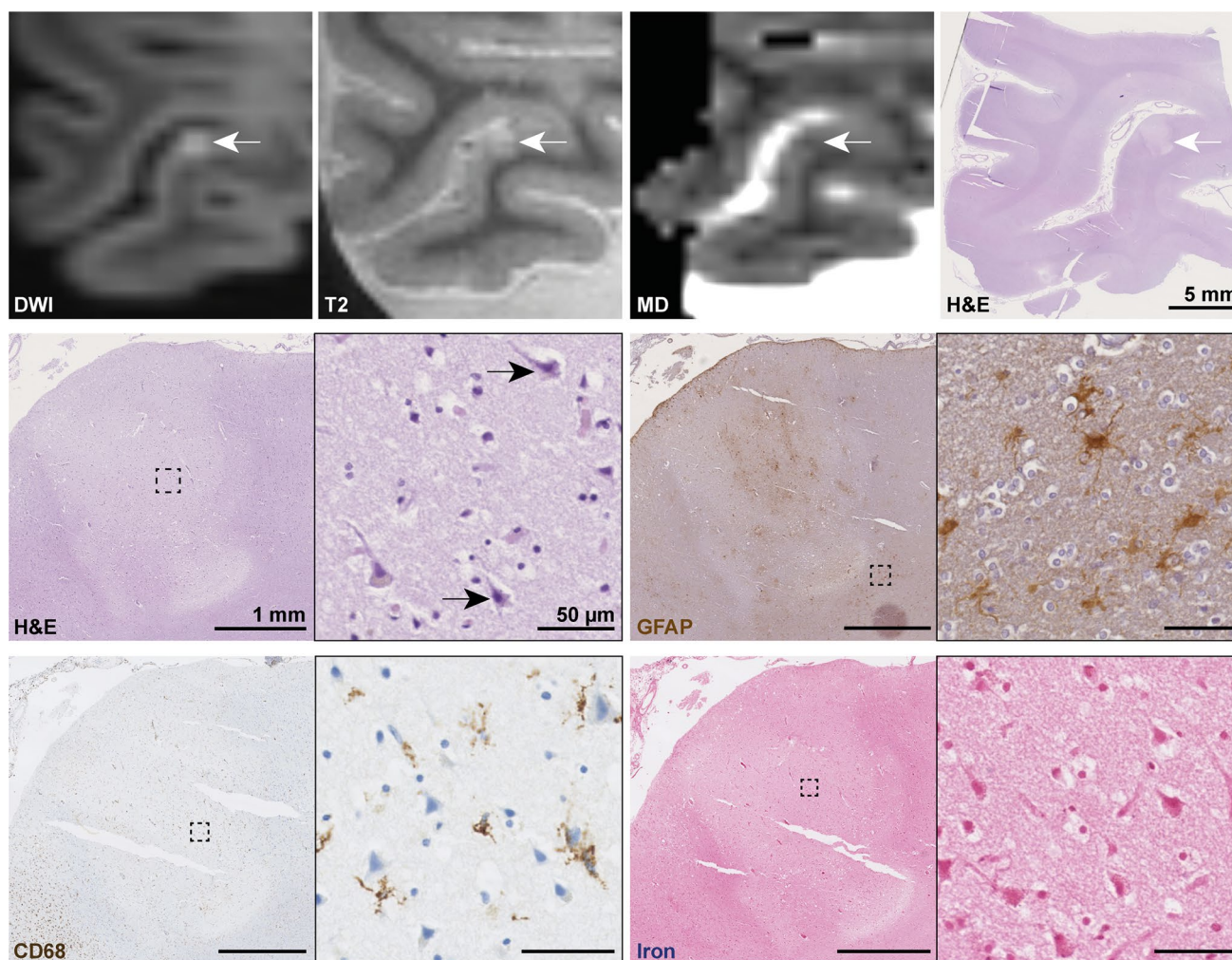


**Fig. 3** Histopathological analysis of an ex vivo DWI+/T2+ lesion confirming acute cortical microinfarct. An ex vivo DWI+/T2+ lesion with corresponding hypointense signal on MD was sampled and successfully retrieved for histopathological analysis (white arrows, scale bar on H&E is 5 mm). On H&E the lesion is marked by a focal area of tissue pallor containing eosinophilic neurons (black arrows inset). The adjacent GFAP stained section revealed only few reactive astrocytes in the lesion periphery (inset) and astrocytic clasmatodendro-

sis within the lesion core. On CD68, a few fragmented microglia were observed. The lesion was negative for iron. Collectively, these pathological features are indicative of an acute cortical microinfarct. Scale bars on sections depicting the lesion are 1 mm, and scale bars in insets are 50  $\mu$ m. *DWI* diffusion-weighted imaging, *MD* mean diffusivity map, *H&E* hematoxylin & eosin, *GFAP* glial fibrillary acidic protein, *CD68* cluster of differentiation 68

of CD68-positive microglia and macrophages, on the basis of which we were able to further specify subacute and chronic cortical microinfarcts in a consensus meeting between the two raters. 8/17 microinfarcts without central cavitation demonstrated a high concentration of amoeboid microglia in the center of the lesion and were, therefore, considered subacute (Fig. 5) [16]. None of the subacute microinfarcts was hyperintense on DWI or T2 1 mm<sup>3</sup>, but four were detectable on T2 0.5 mm<sup>3</sup>. On T2, one subacute microinfarct was hyperintense, whereas the remaining three appeared isointense with the white matter at their core with or without a hyperintense rim (Fig. 5). The remaining 9/17 chronic cortical microinfarcts

either contained amoeboid microglia in combination with a central cavity or contained substantially less or almost no amoeboid microglia (such as shown in Fig. 4). None of these chronic microinfarcts were DWI+. 2/9 chronic microinfarcts were detectable on T2 0.5 mm<sup>3</sup> and 1 mm<sup>3</sup>, with one being hyperintense, and the other one being isointense with the white matter.

When combining MRI-targeted microinfarcts and those detected in retrospect, we observed that acute cortical microinfarcts ( $n = 12$ ) were significantly larger (1.84 mm [1.66–3.10]) compared to subacute/chronic cortical microinfarcts ( $n = 20$ ) as measured on H&E (0.74 mm [0.44–1.27],  $p < 0.001$ ).

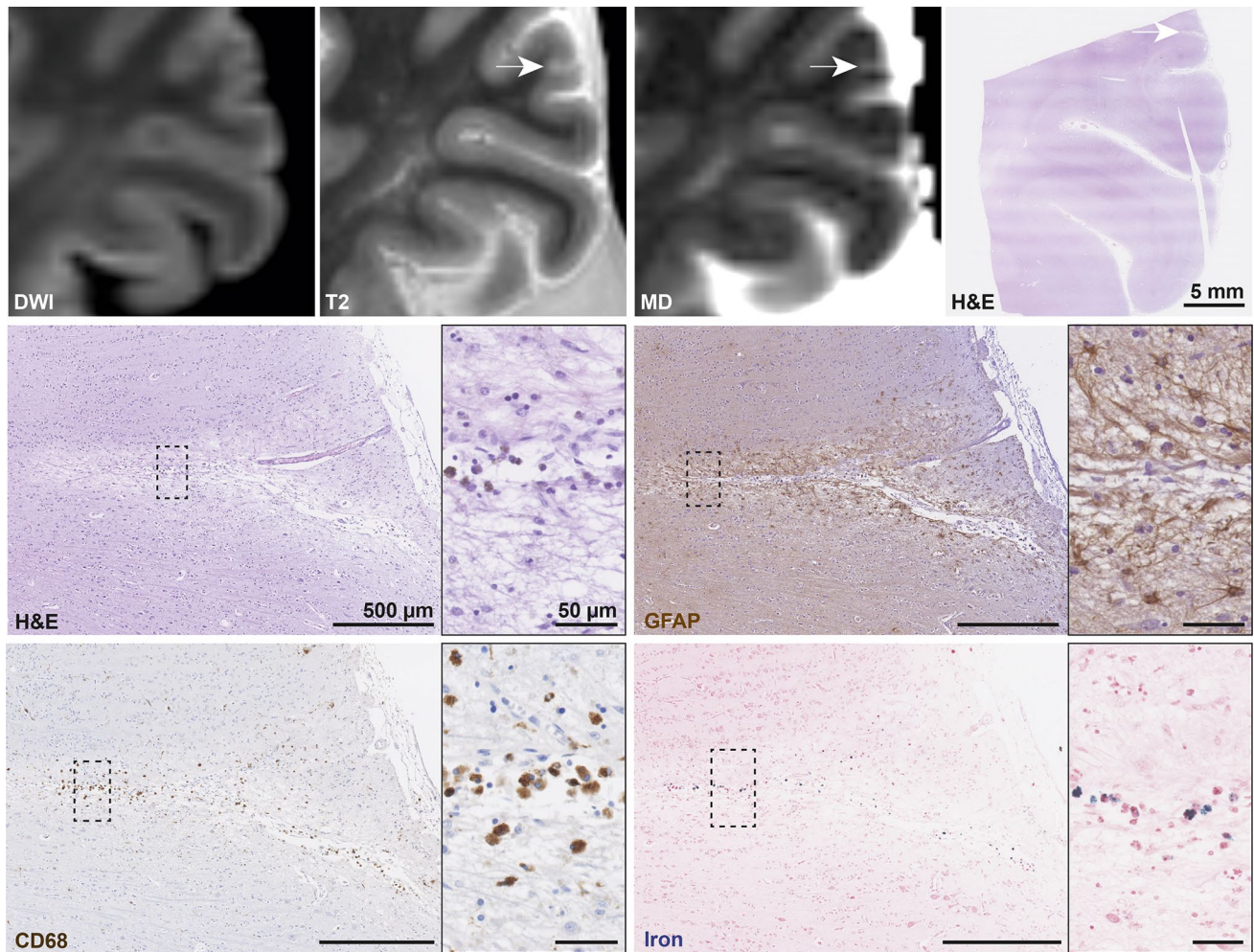


**Fig. 4** Histopathological analysis of an ex vivo DWI-/T2+ lesion confirming chronic cortical microinfarct. An ex vivo DWI-/T2+ lesion with corresponding hyperintense signal on MD was sampled and successfully retrieved for histopathological analysis (white arrows, scale bar on H&E is 5 mm). On H&E the lesion is marked by a focal area of tissue pallor, neuronal loss and cavitation (inset). The adjacent GFAP stained section revealed many reactive astrocytes (astrogliosis) in the lesion periphery (inset). On CD68 only a

few amoeboid microglia were observed. The lesion was mildly positive for iron. Collectively, these pathological features correspond to a chronic cortical microinfarct. Scale bars on sections depicting the lesion are 500  $\mu\text{m}$ , scale bars in insets are 50  $\mu\text{m}$ . *DWI* diffusion-weighted imaging, *MD* mean diffusivity map, *H&E* hematoxylin & eosin, *GFAP* glial fibrillary acidic protein, *CD68* cluster of differentiation 68

### Classification accuracy, and sensitivity and specificity analysis

Next, we assessed the performance of ex vivo DWI regarding the classification and detection of acute cortical microinfarcts. All eight targeted DWI+/T2+ lesions were correctly predicted to represent acute cortical microinfarcts, resulting in a classification accuracy of 100%. Along with these eight true positives, three acute cortical microinfarcts were missed by ex vivo DWI (false negatives), resulting in a sensitivity of 73% (95% CI 39–94%). Last, all 20 chronic cortical microinfarcts were not visible on ex vivo DWI (true negatives:  $n=20$ , false positives:  $n=0$ ), leading to a specificity of 100% (95% CI 83–100%).

### Discussion

The present study, in which we aimed to determine whether small DWI+ lesions represent histopathologically defined acute microinfarcts in the context of CAA, has two key findings. First, using a combined in vivo MRI—ex vivo MRI—histopathology approach we demonstrated that small DWI+ lesions frequently observed in patients with CAA correspond to acute microinfarcts. Furthermore, our data highlight that multimodal ex vivo MRI can be used to distinguish different cortical microinfarct stages in fixed human brain tissue.

Previous human studies and animal experiments have described the histopathological changes following cerebral artery occlusion, which become evident ~6 h post-stroke

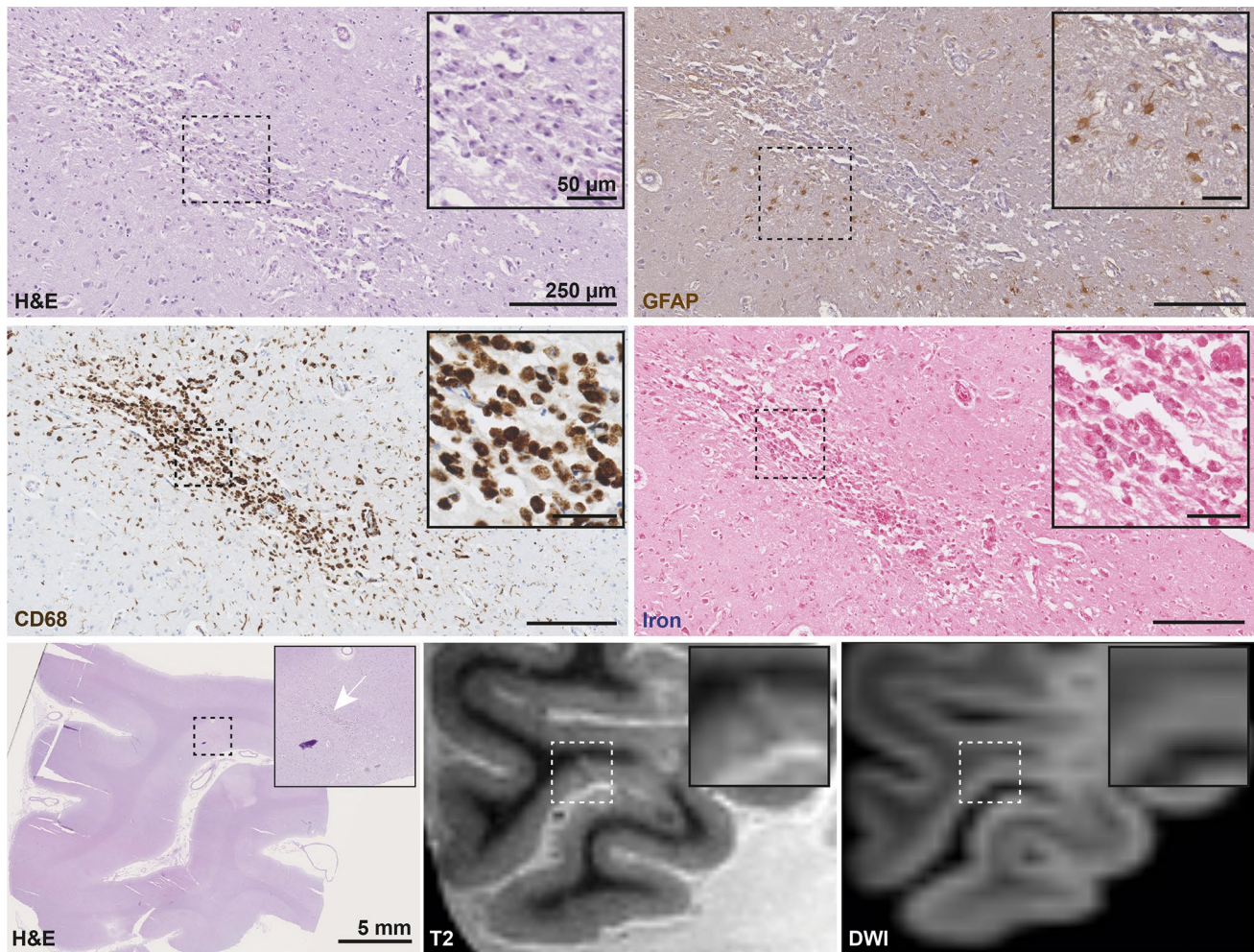


**Fig. 5** MRI features of a histopathologically defined subacute cortical microinfarct. On microscopic examination additional cortical microinfarcts were observed of which a subset was considered subacute. These lesions appeared slit-like or as puckering, without central cavitation and eosinophilic neurons on H&E, but with moderate astrogliosis on GFAP. On CD68, these lesions were characterized by many amoeboid microglia in the core of the lesion. The lesion depicted

here was negative for iron. Importantly, this lesion was matched to a lesion on ex vivo T2 which appeared isointense with the white matter at the lesion core with a hyperintense rim. The lesion was not visible on DWI. Scale bars: on sections depicting the lesion are 250  $\mu$ m, on insets 50  $\mu$ m, and on overview H&E 5 mm. *H&E* hematoxylin & eosin, *GFAP* glial fibrillary acidic protein, *CD68* cluster of differentiation 68, *DWI* diffusion-weighted imaging

[8, 41]. During the acute phase (hours–days) neurons appear shrunken, eosinophilic and pyknotic. This phase is followed by an inflammatory response ( $\geq 3$  days) as evidenced by reactive astrocytes and microglia, and infiltration of macrophages. In the final phase, marked tissue loss is observed, frequently involving a cavitation with a rim of reactive astrocytes, but fewer macrophages [15, 17, 22, 26, 30, 42]. However, histopathological investigations of small subclinical DWI+ lesions were still lacking. Ideally, such a study would require cases with a subclinical DWI+ lesion on (high-resolution) MRI acquired shortly before death, and intact brain tissue subjected to high-resolution ex vivo MRI to guide tissue sampling. Although the prevalence of small DWI+ lesions is increased in CAA, their detection is limited due to their subclinical nature and the normalization of

the DWI scan within the first weeks after lesion onset. As such, our case with CAA and an in vivo DWI+ lesion 7 days prior to death represented a unique situation. The lesion was matched to an area of recent ischemia, although the chance of a false-positive finding was high, owing to the difference in resolution between the in vivo and ex vivo MRI. Our efforts demonstrate the challenges and requirements implicated in the histopathological verification of in vivo small DWI+ lesions, which reflects why such a study on multiple cases has not been performed to date.

As a more reliable and direct way to investigate the histopathology of DWI+ lesions, we evaluated whole hemisphere high-resolution ex vivo MRI scans of CAA cases (and controls) with known microinfarcts [34, 35, 39]. In the current study, we identified a total of 500 cortical

lesions that were hyperintense on ex vivo T2 in 15 cases. In addition, using an ex vivo DWI sequence, we observed that 130/500 (26%) of these lesions were also hyperintense on DWI. To the best of our knowledge the detection of DWI+ lesions in fixed post-mortem human brain tissue has not been reported before. Our targeted histopathological analysis confirmed that the ex vivo DWI+ lesions were acute microinfarcts with 100% specificity.

The finding that ex vivo DWI+ lesions were also detected in a positive control with known in vivo DWI+ lesions shortly before death suggests that DWI retains reliable information on diffusion properties in fixed post-mortem tissue. This is in line with previous ex vivo studies performing successful tractography of white matter tracts based on diffusion imaging of human brains [24, 38]. Unexpectedly, in our study, longer fixation times were positively associated with the number of DWI+/T2+ lesions, which may reflect changes in diffusion properties after prolonged fixation. Previous studies have shown a decrease of T2 relaxation times and the diffusion coefficient after fixation [24]. However, these changes occurred within the first few days within brain areas near the surface and within the first few weeks within deep brain areas, after which both values stabilized [6, 24]. To account for these effects, cerebral hemispheres were scanned after fixation in formalin for at least 4 weeks. In a previous study, fixation duration did not affect associations between diffusion metrics in the white matter and histopathological features (such as myelin density) [38], but the effects of fixation duration on the detectability of ischemic lesions are completely unknown as no prior study addressed DWI+ lesions in an ex vivo study. Since the positive association between fixation duration and ex vivo DWI+ lesions in our study was only based on 12 cases, future longitudinal ex vivo studies in larger datasets are needed to confirm if DWI+ lesions become increasingly visible after prolonged fixation and to explore potential underlying mechanisms for this phenomenon.

Given that DWI+/T2+ lesions had the same topographical distribution as DWI-/T2+ lesions and were correlated with the number of DWI-/T2+ lesions, we suggest that they resemble part of the spectrum of observed microinfarcts in the context of CAA. Whereas the number of DWI+/T2+ lesions on ex vivo MRI was not associated with global CAA severity on histopathology, a recent study reported that microinfarcts were found in areas with increased CAA burden locally [39]. Notably, this was true for both chronic and acute cortical microinfarcts as defined histopathologically. Moreover, in-depth analysis at the single-vessel level identified that vessels involved in both acute and chronic microinfarcts were characterized by severe CAA and loss of smooth muscle cells, likely increasing the risk for ischemia in areas perfused by these presumably dysfunctional vessels [39].

On in vivo MRI, acute infarcts are accompanied by a distinct bright signal on DWI as a result of diffusion restriction due to intracellular cytotoxic edema immediately after infarct onset [25]. Although we did not attempt to explore whether the mechanisms underlying the increased DWI signal in vivo and ex vivo are the same, it appears from our data that the increased concentration of water intracellularly (i.e., cytotoxic edema) is maintained, even after death and fixation of the tissue. It should be noted that the number of detected DWI+ lesions in this post-mortem dataset was much higher than usually observed on in vivo MRI in patients with CAA. DWI+ lesions tended to be negatively associated with post-mortem interval and as such likely occurred pre-mortem or in a limited post-mortem interval. They were also exclusively found in patients with CAA, further suggesting that these lesions are not simply non-specific artifacts related to ex vivo scanning, but rather a feature of advanced SVD. A plausible explanation is that peri-mortem events, such as cerebral hypoperfusion, may have acted as a catalyst for the occurrence of ischemia in areas with severe CAA.

The high sensitivity of ex vivo DWI for the detection of acute cortical microinfarcts suggests that the number of DWI+/T2+ lesions detected on ex vivo MRI is an accurate representation of the total number of acute microinfarcts present in the brain. This is probably due to two important features of acute microinfarcts, which facilitate their detection. First, acute microinfarcts have a distinct bright DWI signal, possibly due to cytotoxic edema. Second, we observed that acute cortical microinfarcts are significantly larger in size compared to subacute/chronic cortical microinfarcts, which increases the likelihood of surpassing the threshold of detectability. The increased DWI signal observed in these lesions did not appear to be driven by T2-shine through effects, since older microinfarcts were not rated as DWI+.

In contrast to acute cortical microinfarcts, microscopic examination of the sections revealed additional older cortical microinfarcts. We further specified these older microinfarcts into subacute and chronic based on the presence of CD68-positive amoeboid microglia covering the lesion core (subacute) or substantially fewer CD68-positive amoeboid microglia with or without a central cavity (chronic). This distinction corresponds well to results of a prior study modeling cerebral microinfarcts in mice that demonstrated a high concentration of CD68-positive microglia at day 3, which gradually decreased until day 28, the point at which some microinfarcts had undergone cavitation [42]. Collectively, we suggest an ante-mortem time frame of hours–days for acute cortical microinfarcts, of days–a few weeks for subacute cortical microinfarcts and of weeks for chronic cortical microinfarcts [15, 17, 22, 26, 30, 42]. In contrast to acute cortical microinfarcts, these older microinfarcts were largely invisible on high-resolution ex vivo MRI suggesting that the total number of microinfarcts present in the brain that have

accumulated over many years remains largely invisible even to high-resolution MRI as noted in previous studies [35, 37, 39]. While this is partly attributable to size, our novel findings extend this notion and suggest that predominantly older subacute or chronic microinfarcts escape detection, whereas acute microinfarcts are more easily visible. In line with this notion are several *in vivo* studies in humans and mice that investigated the evolution of acute DWI+ lesions and demonstrated disappearance of a subset of these lesions on follow-up MRI [5, 11, 32, 33, 36, 43]. Two experimental studies in mice showed that microinfarcts were largest between day 1–3 after vessel occlusion and shrank thereafter, possibly reflective of histologic evolution of the acute infarct and/or tissue collapse [32, 42]. Remarkably, we noted that subacute microinfarcts, that had not undergone cavitation, were rather inconspicuous on MRI. Collectively, our data may provide a mechanistic framework for the observation of disappearing DWI+ lesions on follow-up *in vivo* MRI and suggest that when microinfarcts evolve, T2-based imaging sequences may favor the detection of larger microinfarcts that underwent cavitation, while being insensitive to the smaller and subacute subset. These observations have two implications. First, future—preferably longitudinal—studies are needed to determine if the current rating criteria for microinfarcts on MRI need to be modified to benefit the accurate detection of the subacute subset [37]. Second, because of lesion shrinkage over time, the 100% specificity of *ex vivo* DWI for the detection of acute microinfarcts observed in the current study may have been driven by microinfarct size as most chronic microinfarcts failed to pass the detection limit of the 1.0 mm<sup>3</sup> DWI scan.

This study has several important clinical implications. First, CAA is a major risk factor for ICH, but is also associated with a high prevalence of DWI+ lesions and thus acute ischemia, within as well as beyond the acute ICH window. This poses challenges to clinicians who must weigh the risks of future hemorrhagic or ischemic events when deciding on treatment strategies after ICH, including aggressive blood pressure reduction in the acute ICH period, and use or avoidance of antithrombotics [2, 23, 27]. Second, DWI+ lesions also occur in other types of SVD and our findings on the ischemic nature of DWI+ lesions can likely be generalized to these conditions [33, 43]. Recently, it was shown that small subclinical DWI+ lesions are associated with poor clinical outcome after 2-year follow-up in memory clinic patients with vascular disease on MRI [7]. Hence, prevention of acute ischemia in the elderly seems to be an important target for clinicians. Last, we demonstrate that it is possible to define microinfarct age with multimodal *ex vivo* MRI, which may benefit histopathological studies investigating the etiology of microvascular lesions [39]. As histopathology studies are inherently cross-sectional, cause–effect relationships cannot be inferred. Yet, comparing the histopathological

features of acute and chronic microvascular lesions may provide new hypotheses on lesion etiology [39], and the present study demonstrates that using post-mortem MRI it is possible to target acute, subacute and chronic cortical microinfarcts directly.

The present study provides the first comprehensive assessment of the histopathological nature of small DWI+ lesions. Yet, several important limitations should be addressed. First, this study provided extensive evidence that the small DWI+ lesions seen on *ex vivo* MRI are indeed acute microinfarcts, but limited evidence for the lesions seen on *in vivo* MRI. While we show that demonstrating this association is highly challenging in human studies, it could be achieved in animal models [29]. Second, no detailed information was collected regarding peri-mortem events for each case, which may have influenced occurrence of acute ischemia, as discussed above. Third, our results on the mean diffusivity remain exploratory, since we could not generate a reliable mean diffusivity map based on the steady-state free precession diffusion sequence, due to absence of a quantitative T2 map [21]. Fourth, the resolution of the *ex vivo* DWI sequence did not match the T2 sequence. To account for this limitation, we down sampled the T2 scan to a 1 mm<sup>3</sup> resolution and only targeted DWI–/T2+ lesions for histopathology that were also visible on the down sampled T2 scan. This approach may have resulted in a selection bias, as the DWI–/T2+ lesions that remained detectable on the down sampled T2 scans corresponded mostly to larger cavitated chronic microinfarcts with a distinct hyperintense signal. We cannot exclude the possibility that some of the extra subacute/chronic microinfarcts that were detected in the retrospective analysis may have been DWI+ but too small to be visible on the 1 mm<sup>3</sup> scans. Fifth, although the histopathological features of microinfarcts were strongly suggestive of primary ischemia, inherent to *ex vivo* analyses we cannot entirely rule out that some microinfarcts may have had a hemorrhagic origin. Furthermore, we purposely only screened the cerebral cortex for the presence of microinfarcts to allow comparison with a previous study [39]. Since microinfarcts also occur in the subcortical white matter [31], future studies are needed to systematically assess the detection of subcortical microinfarcts on MRI. Finally, four lesions were lost for histopathological examination due to erroneous sampling, which reflects the technical challenges of MRI—histopathology studies, especially when going directly from whole hemispheres to histological sections. Subjecting individual formalin-fixed cut slabs to ultra-high-resolution scanning as an intermediate step improves sampling strategies of targeted lesions [35, 39].

In conclusion, we suggest that small DWI+ lesions in CAA represent acute microinfarcts. Furthermore, our findings support the use of *ex vivo* DWI as a method to detect acute microinfarcts post-mortem, which may benefit

future histopathological investigations on the etiology of microinfarcts.

**Acknowledgements** The authors would like to thank the families of the patients who generously donated their brains to our research studies. The authors would also like to thank Dr. Ana Amaral and Dr. Patrick Dooley for their excellent technical assistance and Dr. Alberto Serrano-Pozo for helpful discussions. The work described in this study was supported by the Van Leersum Grant of the Royal Netherlands Academy of Arts and Sciences and an Alzheimer Nederland fellowship to AtT, and the National Institutes of Health (NINDS R01 NS096730, NIA K99 AG059893, NINDS RF1 NS110054, and NIA R21 AG046657). During this study, SJvV received funding from the Netherlands Organisation for Scientific Research (Veni Grant 91619021). MD received funding from the Radboud Excellence Initiative (18U.018651). FEDL was supported by a clinical established investigator grant of the Dutch Heart Foundation (Grant 2014 T060), and by a VIDI innovational grant from The Netherlands Organisation for Health Research and Development, ZonMw (Grant 016126351).

## References

- Arvanitakis Z, Capuano AW, Leurgans SE, Buchman AS, Bennett DA, Schneider JA (2017) The relationship of cerebral vessel pathology to brain microinfarcts. *Brain Pathol* 27:77–85. <https://doi.org/10.1111/bpa.12365>
- Auriel E, Gurol ME, Ayres A, Dumas AP, Schwab KM, Vashkevich A et al (2012) Characteristic distributions of intracerebral hemorrhage-associated diffusion-weighted lesions. *Neurology* 79:2335–2341. <https://doi.org/10.1212/WNL.0b013e318278b66f>
- Batool S, O'Donnell M, Sharma M, Islam S, Dagenais GR, Poirier P et al (2014) Incidental magnetic resonance diffusion-weighted imaging-positive lesions are rare in neurologically asymptomatic community-dwelling adults. *Stroke* 45:2115–2117. <https://doi.org/10.1161/strokeaha.114.005782>
- Dale AM, Fischl B, Sereno MI (1999) Cortical surface-based analysis: I. Segmentation and surface reconstruction. *Neuroimage* 9:179–194
- Duering M, Adam R, Wollenweber FA, Bayer-Karpinska A, Baykara E, Cubillos-Pinilla LY et al (2019) Within-lesion heterogeneity of subcortical DWI lesion evolution, and stroke outcome: a voxel-based analysis. *J Cereb Blood Flow Metab*. <https://doi.org/10.1177/0271678x19865916>
- Dyrby TB, Baare WF, Alexander DC, Jelsing J, Garde E, Sogaard LV (2011) An ex vivo imaging pipeline for producing high-quality and high-resolution diffusion-weighted imaging datasets. *Hum Brain Mapp* 32:544–563. <https://doi.org/10.1002/hbm.21043>
- Ferro DA, van den Brink H, Exalto LG, Boomsma JM, Barkhof F, Prins ND et al (2019) Clinical relevance of acute cerebral microinfarcts in vascular cognitive impairment. *Neurology* 92:e1558–e1566
- Garcia JH, Yoshida Y, Chen H, Li Y, Zhang ZG, Lian J et al (1993) Progression from ischemic injury to infarct following middle cerebral artery occlusion in the rat. *Am J Pathol* 142:623–635
- Greenberg SM, Charidimou A (2018) Diagnosis of cerebral amyloid angiopathy: evolution of the Boston criteria. *Stroke* 49:491–497. <https://doi.org/10.1161/strokeaha.117.016990>
- Gregoire SM, Charidimou A, Gadapa N, Dolan E, Antoun N, Peeters A et al (2011) Acute ischaemic brain lesions in intracerebral haemorrhage: multicentre cross-sectional magnetic resonance imaging study. *Brain* 134:2376–2386. <https://doi.org/10.1093/brain/awr172>
- Havsteen I, Ovesen C, Willer L, Nybing JD, Aegidius K, Marstrand J et al (2018) Small cortical grey matter lesions show no persistent infarction in transient ischaemic attack? A prospective cohort study. *BMJ Open* 8:e018160
- Hilal S, Baaij LGA, de Groot M, Niessen WJ, Ikram MK, Ikram MA et al (2019) Prevalence and clinical relevance of diffusion-weighted imaging lesions: the Rotterdam study. *Neurology* 93:e1058–e1067. <https://doi.org/10.1212/wnl.00000000000008090>
- Hyman BT, Phelps CH, Beach TG, Bigio EH, Cairns NJ, Carrillo MC et al (2012) National Institute on Aging-Alzheimer's Association guidelines for the neuropathologic assessment of Alzheimer's disease. *Alzheimer's Dement* 8:1–13. <https://doi.org/10.1016/j.jalz.2011.10.007>
- Jenkinson M, Bannister P, Brady M, Smith S (2002) Improved optimization for the robust and accurate linear registration and motion correction of brain images. *Neuroimage* 17:825–841
- Jeon JH, Jung HW, Jang HM, Moon JH, Park KT, Lee HC et al (2015) Canine model of ischemic stroke with permanent middle cerebral artery occlusion: clinical features, magnetic resonance imaging, histopathology, and immunohistochemistry. *J Vet Sci* 16:75–85
- Karperien A, Ahammer H, Jelinek HF (2013) Quantitating the subtleties of microglial morphology with fractal analysis. *Front Cell Neurosci* 7:3. <https://doi.org/10.3389/fncel.2013.00003>
- Kelly PJ, Hedley-Whyte ET, Primavera J, He J, Gonzalez RG (2001) Diffusion MRI in ischemic stroke compared to pathologically verified infarction. *Neurology* 56:914–920. <https://doi.org/10.1212/wnl.56.7.914>
- Kimberly WT, Gilson A, Rost NS, Rosand J, Viswanathan A, Smith EE et al (2009) Silent ischemic infarcts are associated with hemorrhage burden in cerebral amyloid angiopathy. *Neurology* 72:1230–1235. <https://doi.org/10.1212/01.wnl.0000345666.83318.03>
- Leemans A, Jeurissen B, Sijbers J, Jones D (2009) ExploreDTI: a graphical toolbox for processing, analyzing, and visualizing diffusion MR data. In: Proceedings of the international society for magnetic resonance in medicine, p 3537
- Love S, Chalmers K, Ince P, Esiri M, Attems J, Jellinger K et al (2014) Development, appraisal, validation and implementation of a consensus protocol for the assessment of cerebral amyloid angiopathy in post-mortem brain tissue. *Am J Neurodegener Dis* 3:19–32
- McNab JA, Jbabdi S, Deoni SC, Douaud G, Behrens TE, Miller KL (2009) High resolution diffusion-weighted imaging in fixed human brain using diffusion-weighted steady state free precession. *Neuroimage* 46:775–785. <https://doi.org/10.1016/j.neuroimage.2009.01.008>
- Mena H, Cadavid D, Rushing EJ (2004) Human cerebral infarct: a proposed histopathologic classification based on 137 cases. *Acta Neuropathol* 108:524–530. <https://doi.org/10.1007/s00401-004-0918-z>
- Menon RS, Burgess RE, Wing JJ, Gibbons MC, Shara NM, Fernandez S et al (2012) Predictors of highly prevalent brain ischemia in intracerebral hemorrhage. *Ann Neurol* 71:199–205. <https://doi.org/10.1002/ana.22668>
- Miller KL, Stagg CJ, Douaud G, Jbabdi S, Smith SM, Behrens TEJ et al (2011) Diffusion imaging of whole, post-mortem human brains on a clinical MRI scanner. *Neuroimage* 57:167–181. <https://doi.org/10.1016/j.neuroimage.2011.03.070>
- Minematsu K, Li L, Fisher M, Sotak CH, Davis MA, Fiandaca M (1992) Diffusion-weighted magnetic resonance imaging: rapid and quantitative detection of focal brain ischemia. *Neurology* 42:235
- Okamoto Y, Ihara M, Fujita Y, Ito H, Takahashi R, Tomimoto H (2009) Cortical microinfarcts in Alzheimer's disease and subcortical vascular dementia. *NeuroReport* 20:990–996

27. RESTART Collaboration (2019) Effects of antiplatelet therapy after stroke due to intracerebral haemorrhage (RESTART): a randomised, open-label trial. *Lancet* 393:2613–2623. [https://doi.org/10.1016/s0140-6736\(19\)30840-2](https://doi.org/10.1016/s0140-6736(19)30840-2)
28. Schulz UG, Flossmann E, Francis JM, Redgrave JN, Rothwell PM (2007) Evolution of the diffusion-weighted signal and the apparent diffusion coefficient in the late phase after minor stroke: a follow-up study. *J Neurol* 254:375–383. <https://doi.org/10.1007/s00415-006-0381-y>
29. Shih AY, Hyacinth HI, Hartmann DA, van Veluw SJ (2018) Rodent models of cerebral microinfarct and microhemorrhage. *Stroke* 49:803–810. <https://doi.org/10.1161/strokeaha.117.016995>
30. Smith EE, Schneider JA, Wardlaw JM, Greenberg SM (2012) Cerebral microinfarcts: the invisible lesions. *Lancet Neurol* 11:272–282. [https://doi.org/10.1016/s1474-4422\(11\)70307-6](https://doi.org/10.1016/s1474-4422(11)70307-6)
31. Soontornniyomkij V, Lynch MD, Mermash S, Pomakian J, Badkoobehi H, Clare R et al (2010) Cerebral microinfarcts associated with severe cerebral beta-amyloid angiopathy. *Brain Pathol* 20:459–467. <https://doi.org/10.1111/j.1750-3639.2009.00322.x>
32. Summers PM, Hartmann DA, Hui ES, Nie X, Deardorff RL, McKinnon ET et al (2017) Functional deficits induced by cortical microinfarcts. *J Cereb Blood Flow Metab*. <https://doi.org/10.1177/0271678x16685573>
33. ter Telgte A, Wiegertjes K, Gesierich B, Marques JP, Huebner M, de Klerk JJ et al (2019) Contribution of acute infarcts to cerebral small vessel disease progression. *Ann Neurol* 86:582–592. <https://doi.org/10.1002/ana.25556>
34. van Veluw SJ, Zwanenburg JJ, Engelen-Lee J, Spliet WG, Hendrikse J, Luijten PR et al (2013) In vivo detection of cerebral cortical microinfarcts with high-resolution 7T MRI. *J Cereb Blood Flow Metab* 33:322–329. <https://doi.org/10.1038/jcbfm.2012.196>
35. van Veluw SJ, Charidimou A, van der Kouwe AJ, Lauer A, Reijmer YD, Costantino I et al (2016) Microbleed and microinfarct detection in amyloid angiopathy: a high-resolution MRI-histopathology study. *Brain* 139:3151–3162. <https://doi.org/10.1093/brain/aww229>
36. van Veluw SJ, Lauer A, Charidimou A, Bounemia N, Xiong L, Boulouis G et al (2017) Evolution of DWI lesions in cerebral amyloid angiopathy: evidence for ischemia. *Neurology* 89:2136–2142. <https://doi.org/10.1212/wnl.0000000000004668>
37. van Veluw SJ, Shih AY, Smith EE, Chen C, Schneider JA, Wardlaw JM et al (2017) Detection, risk factors, and functional consequences of cerebral microinfarcts. *Lancet Neurol* 16:730–740. [https://doi.org/10.1016/s1474-4422\(17\)30196-5](https://doi.org/10.1016/s1474-4422(17)30196-5)
38. van Veluw SJ, Reijmer YD, van der Kouwe AJ, Charidimou A, Riley GA, Leemans A et al (2019) Histopathology of diffusion imaging abnormalities in cerebral amyloid angiopathy. *Neurology* 92:e933–e943. <https://doi.org/10.1212/wnl.0000000000007005>
39. van Veluw SJ, Scherlek AA, Freeze WM, ter Telgte A, van der Kouwe AJ, Bacskai BJ et al (2019) Different microvascular alterations underlie microbleeds and microinfarcts. *Ann Neurol* 86:279–292. <https://doi.org/10.1002/ana.25512>
40. Viswanathan A, Greenberg SM (2011) Cerebral amyloid angiopathy in the elderly. *Ann Neurol* 70:871–880. <https://doi.org/10.1002/ana.22516>
41. von Kummer R, Dzialowski I (2017) Imaging of cerebral ischemic edema and neuronal death. *Neuroradiology* 59:545–553. <https://doi.org/10.1007/s00234-017-1847-6>
42. Wang M, Iliff JJ, Liao Y, Chen MJ, Shinseki MS, Venkataraman A et al (2012) Cognitive deficits and delayed neuronal loss in a mouse model of multiple microinfarcts. *J Neurosci* 32:17948–17960. <https://doi.org/10.1523/jneurosci.1860-12.2012>
43. Wiegertjes K, ter Telgte A, Oliveira PB, van Leijns EMC, Bergkamp MI, van Uden IWM et al (2019) The role of small diffusion-weighted imaging lesions in cerebral small vessel disease. *Neurology*. <https://doi.org/10.1212/wnl.0000000000008364>

**Publisher's Note** Springer Nature remains neutral with regard to jurisdictional claims in published maps and institutional affiliations.